Journal of Power Sources 191 (2009) 58–75

Contents lists available at ScienceDirect

Journal of Power Sources

journal homepage: www.elsevier.com/locate/jpowsour

Mechanism of action of electrochemically active carbons on the processes that take place at the negative plates of lead-acid batteries

D. Pavlov*, T. Rogachev, P. Nikolov, G. Petkova

Institute of Electrochemistry and Energy Systems, Bulgarian Academy of Sciences, Acad. G. Bonchev Street, bl. 10, Sofia 1113, Bulgaria

ARTICLE INFO

Article history:
Received 30 September 2008
Received in revised form 6 November 2008
Accepted 7 November 2008
Available online 24 November 2008

Keywords:
Active carbon
Lead-acid battery
Negative active material
Valve-regulated lead-acid
High-rate partial-state-of-charge
Cycle-life

ABSTRACT

It is known that negative plates of lead-acid batteries have low charge acceptance when cycled at high rates and progressively accumulate lead sulphate on high-rate partial-state-of-charge (HRPSoC) operation in hybrid-electric vehicle (HEV) applications. Addition of some carbon or graphite forms to the negative paste mix improves the charge efficiency and slows down sulfation of the negative plates. The present investigation aims to elucidate the contribution of electrochemically active carbon (EAC) additives to the mechanism of the electrochemical reactions of charge of the negative plates. Test cells are assembled with four types of EAC added to the negative paste mix in five different concentrations. Through analysis of the structure of NAM (including specific surface and pore radius measurements) and of the electrochemical parameters of the test cells on HRPSoC cycling, it is established that the electrochemical reaction of charge $Pb^{2+} + 2e^- \rightarrow Pb$ proceeds at 300–400 mV lower over-potentials on negative plates doped with EAC additives as compared to the charge potentials of cells with no carbon additives. Hence, *electrochemically active carbons have a highly catalytic effect on the charge reaction and are directly involved in it*. Consequently, the reversibility of the charge/discharge processes is improved, which eventually leads to longer battery cycle life. Thus, charging of the negative plates proceeds via a *parallel mechanism on the surfaces of both Pb and EAC particles*, at a higher rate on the EAC phase. Cells with EAC in NAM have the longest cycle life when their NAM specific surface is up to 4 $m^2 g^{-1}$ against 0.5 $m^2 g^{-1}$ for the lead surface. The proposed parallel mechanism of charge is verified experimentally on model Pb/EAC/$PbSO_4$ and Pb/EAC electrodes. During the charge and discharge cycles of the HRPSoC test, the EAC particles are involved in *dynamic* adsorption/desorption on the lead sulfate and lead surfaces. Another effect of electrochemically active carbons is also evidenced namely that, above a definite concentration, some EAC forms reduce the mean pore radius of NAM. When it diminishes to less than 1.5 μm, access of sulfuric acid into the pores is impeded and PbO forms instead of $PbSO_4$ in the pores of NAM during discharge. Thus, it may be presumed that electrochemically active carbons change the overall electrochemical reaction of charge and discharge of lead-acid cells when operated under HRPSoC cycling conditions.

1. Introduction

Operation of valve-regulated lead-acid batteries (VRLABs) under high-rate partial-state-of-charge (HRPSoC) conditions leads to progressive accumulation of $PbSO_4$ on the negative plates, which limits the cycle life of the batteries. Nakamura, Shiomi and co-authors [1,2] have established that introduction of carbon black to the negative active material retards substantially the sulfation of the negative plates during the simulated HRPSoC test of batteries for hybrid-electric vehicle (HEV) applications. Later, Hollenkamp et al. [3] have studied the build up of $PbSO_4$ on the negative plates by subjecting batteries to simulated HEV cycling at 2*C* rate for 3–4 cycle-sets between 50% and 100% DOD. One cycle-set comprised cycling until pre-set upper limit (e.g. end-of-charge voltage of 2.83 V per cell) and lower limit (e.g. end-of-discharge voltage of 1.83 V per cell) is reached. The batteries were set to capacity-recovery charging (to 100% SoC) and then the next HEV cycle-set followed. After 3–4 cycle-sets the negative plates were irreversibly sulfated and the batteries reached their end-of-life [4]. Newnham et al. [5] have found that the specific surface area of NAM is an important parameter as it sustains the potential of the negative plates below the hydrogen evolution potential. However, not all carbon forms that increase the specific surface of NAM contribute to improvement of battery cycle life on HRPSoC operation.

Moseley et al. [4] have summarized the hypotheses proposed in the literature for the action of carbons on the HRPSoC performance of the batteries as follows: (a) carbon enhances the overall conductivity of NAM [1,3]; (b) carbon facilitates the formation of

* Corresponding author. Tel.: +359 2 9710083; fax: +359 2 8731552.
E-mail address: dpavlov@labatscience.com (D. Pavlov).

0378-7753/$ – see front matter © 2008 Elsevier B.V. All rights reserved.
doi:10.1016/j.jpowsour.2008.11.056

small isolated $PbSO_4$ particles easy to dissolve and restricts $PbSO_4$ crystal growth [2]; (c) some carbon forms contain impurities which impede the reaction of hydrogen evolution and hence improve the efficiency of charge [6,7]; (d) carbon acts as an electro-osmotic pump that facilitates acid diffusion in the inner NAM volume at the high rates of charge and discharge [7]. Lam and co-authors have created the ultra battery with a conventional PbO_2 positive plate and a negative plate comprising two parts: half of it is a carbon electrode and the other half is a regular negative plate (with sponge lead active material [8,9]. In the ultra battery design, carbon is in electrical, but not in physical contact with the negative active material. It has been speculated that only those mechanisms of carbon action which could still operate when the carbon is isolated from the lead active mass can be considered as candidates for providing the major benefit to charge efficiency and impeding negative plate sulfation [6].

Each of the above-mentioned mechanisms exerts its influence on the charge acceptance of negative plates containing carbon and/or graphite additives.

The cycle life of the batteries is determined by the degree of reversibility of the processes that proceed during charge and discharge. In HRPSoC duty the cycle life of the battery is limited by the low charge acceptance of the negative plates. Charging of the negative plates proceeds through the following elementary processes:

- Dissolution of $PbSO_4$ crystals.
- Diffusion of the formed Pb^{2+} ions to the metal surface.
- Electron transfer from the metal surface to Pb^{2+} ions and formation of Pb atoms.
- Surface diffusion of Pb atoms to lead growth fronts and incorporation of these atoms into the growing Pb crystal lattice.

If any of the above elementary processes is impeded, the whole charge process is retarded and certain amounts of $PbSO_4$ in the plates are not reduced to Pb within the programmed charging time. Consequently, lead sulfate accumulates in the plates. Processes of recrystallization occur yielding big $PbSO_4$ crystals difficult to dissolve, which eventually leads to sulfation of the negative plates of lead-acid cells.

The aim of the present investigation was to establish the effect of various types of carbons, added to the negative active material in different concentrations, on the electrochemical reactions of charge of VRLA cells in HRPSoC duty. The cycle life performance of the test cells was evaluated in correlation with the specific surface area and the median pore radius of the formed NAM. These experiments aimed at disclosing the mechanism(s) by which carbon additives are involved in the electrochemical processes of charge of the negative plates in HRPSoC duty.

2. Experimental

2.1. Carbon forms added to the negative active mass

To be able to contribute to the electrochemical reactions of charge, the carbon material added to the negative plate should have the following characteristics:

(a) *High electroconductivity*, which would make the interface carbon/solution electrochemically active and would allow the electrochemical reactions to proceed at this interface.
(b) *High surface area*, which is achieved when the carbon particles are of nano-sizes or porous.
(c) *Strong adhesion to the lead surface*, which would ensure good contact between carbon and lead particles with low ohmic resistance of the carbon/lead interface.

For the purpose of the present investigation we selected four types of commercially available carbon materials, which meet the above requirements for "electrochemically active carbons" (labelled as EAC further in the text). The basic characteristics of the selected EAC are summarized in Table 1. As evident from the table, NORIT AZO is an activated carbon, whereas VULCAN XC72R, Black Pearls 2000 and PRINTEX® XE2 are carbon blacks.

In an attempt to disclose the mechanism(s) by which EAC additives improve the charge acceptance of the negative plates and extend the cycle life of lead-acid cells operated under HRPSoC regime we studied the *influence of carbon concentration* in NAM on the electrochemical behaviour of the negative plates and on the performance of the test cells. Negative plates were prepared with each type of EAC selected for the investigation, varying its amount in 5 different concentrations, and these plates were tested. In this way we varied the electrochemically active surface area of NAM and followed the resultant changes in the electrochemical parameters of the negative plates of lead-acid cells cycled under HRPSoC conditions.

2.2. Test lead-acid cells

2.2.1. Negative paste preparation

The negative pastes were prepared using H_2SO_4 (1.4 sp.gr.) and leady oxide (LO) in 4.5 wt.% ratio. The degree of oxidation of the LO was 76%. Barton oxide from battery plant "Monbat", Bulgaria, was used. The expander formulation was: 0.2% Vanisperse A, 0.8% $BaSO_4$ and EAC additives varying in the range from 0.2% to 2%. A batch of paste without carbon was also prepared and used for assembling a reference cell. All effects of the addition of different types of EAC are discussed in comparison to the reference cell with no carbon. A total of 21 different paste batches were prepared. These pastes were used for production of negative plates for the test cells.

The pasted plates were cured under the following conditions:

- 48 h at 35 °C and 98% relative humidity, followed by
- 24 h at 60 °C and 10% relative humidity.

All plates were formed under identical conditions: in H_2SO_4 (1.06 sp.gr.) for 18 h, employing a formation algorithm developed in this laboratory. The formation process was completed with twice higher quantity of electricity than the theoretical capacity of the plates. After formation, samples of the negative active material were characterized by XRD, chemical analysis, BET surface measurements, mercury porosimetry and SEM examinations.

Table 1
Activated carbons under investigation.

Product	Manufacturer	Type of material	Signature	Specific characteristics:	
				Particle Size	BET surface ($m^2\ g^{-1}$)
NORIT AZO	NORIT	Activated carbon	EAC1	100 μm	635
VULCAN XC72R	Cabot Corporation	Carbon black	EAC2	30 nm	257
Black Pearls 2000	Cabot Corporation	Carbon black	EAC3	12 nm	1475
PRINTEX® XE2	Degussa	Carbon black	EAC4	30 nm	910

Fig. 1. Photograph of a 2 V/4.5 Ah test cell.

2.2.2. Test cell design

The influence of carbon additives on the performance of lead-acid cells was investigated using 4.5 Ah cells with 2 negative and 3 positive plates per cell. The test cell design is presented in Fig. 1 and its characteristics are summarized in Table 2.

The performance parameters of the test cells were limited by the negative plates. Small sized plates with thick grid bars were used to rule out the influence of plate size on cell performance. AGM separators (H&V, USA) with a thickness of 3 mm (425 g m^{-2}) were used at 20% compression. The cells were filled with 75 ml of H_2SO_4 of 1.28 sp.gr. (the electrolyte forming a "mirror" over the plates) and sealed. The rated capacity of the cells at 20 h discharge rate, C_0, was calculated at 50% utilization of the negative active material.

2.3. Electrical parameters of the test cells

2.3.1. Initial cell capacity

The initial capacity of the cells was determined at a discharge current of $I = C_0/20A$. Each cell was subjected to three subsequent capacity tests at 25 °C.

Table 2
Test cell design characteristics.

	Negative plate	Positive plate
Grid alloy (wt.%)	Pb–0.04Ca–1.1Sn	Pb–0.04Ca–1.1Sn
Grid thickness (mm)	1.5	1.5
Grid dimensions (mm)	57 × 60	57 × 60
Plate per cell	2	3
Plate thickness (mm)	2.0	2.5

2.3.2. Peukert dependences

The Peukert dependences were obtained at $C/20$, $C/10$, $C/7$, $C/5$, $C/3$, $C/1$ and $2C$ rates. Charging was conducted in two steps: first step $I_{ch} = 0.5C_0A$ to a voltage limit of 2.45 V, and second step $I_{ch} = 0.2C_0A$

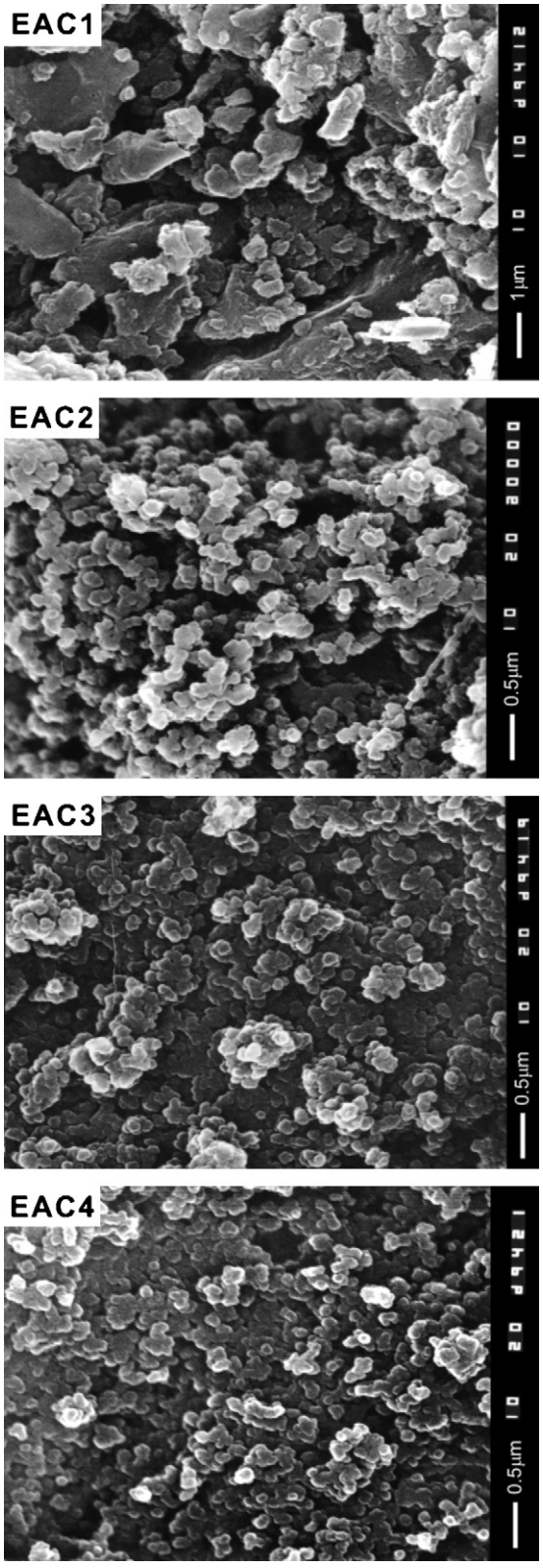

Fig. 2. SEM pictures of samples of the electrochemically active carbon powders (EAC1, EAC2, EAC3 and EAC4) used for the investigations.

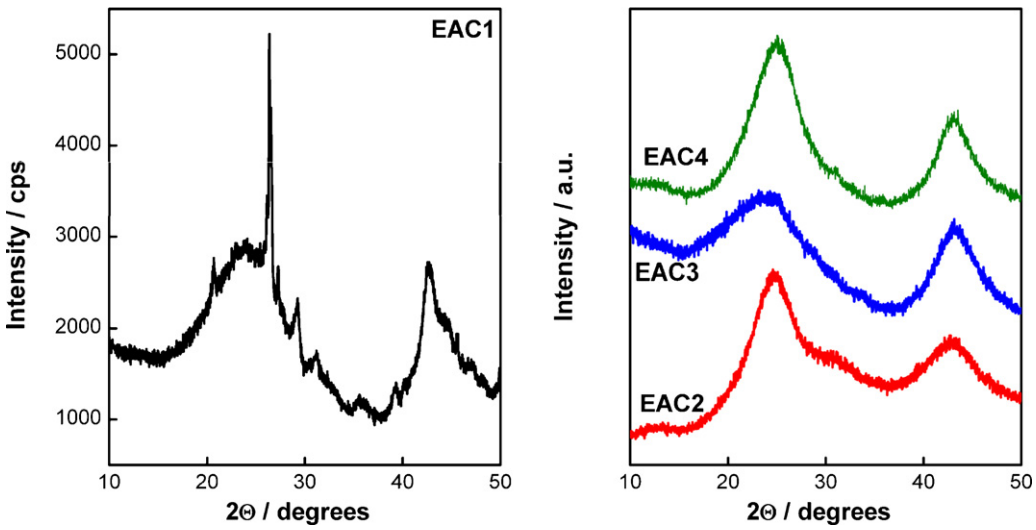

Fig. 3. XRD patterns for electrochemically active carbons EAC1, EAC2, EAC3 and EAC4. All four carbon materials are amorphous. EAC1 contains a crystal component.

to 120% overcharge. The rest period after charge was 30 min. All cell tests were performed using Bitrode testing equipment. The time for discharge to 1.83 V was measured for all testing currents. From the obtained Peukert curves the coefficients n and K for the Peukert equation $K = I^n t$ were calculated. The Peukert dependence was used to determine the 2C cycling current for the HRPSoC tests.

2.3.3. Cycle life test under simulated HRPSoC regime

The effect of carbon materials on cell performance under simulated HRPSoC conditions was evaluated using a simplified profile imitating the micro-hybrid driving mode. The first step in this cycling profile was discharge at $I = 1C$ A rate to 50% SoC (C is the capacity after 1 h discharge determined from the Peukert dependence). After that, the cells were subjected to cycling according to the following schedule: charge at 2C rate for 60 s, rest for 10 s, discharge at 2C rate for 60 s, rest for 10 s. During these tests, the negative plates were cycled between 50% and 53% SoC. The cell voltage was measured at the end of the charge or discharge pulses and the test was stopped when the cell voltage fell down to 1.83 V or when the upper voltage limit of 2.83 V was reached. The above-described cycling steps comprise one cycle-set. If the cell is fully re-charged (to 100% SoC) after this cycle-set, it can endure several more cycle-sets. Let us call conditionally the first cycle-set "cycle life" of the cell. After completing the HRPSoC cycle life test (first cycle-set) the cells were subjected to teardown analysis.

3. Experimental results and discussion

3.1. Characterization of carbon samples

3.1.1. Scanning electron microscopy of electrochemically active carbons

Fig. 2 presents SEM micrographs of samples of the electrochemically active carbons (EACs) used for the investigation.

The EAC1 particles form the largest aggregates (1–2 μm), anisometric in shape. The particles of EAC2, EAC3 and EAC4 are equi-axed with diameters of 80–150 nm.

3.1.2. Crystal structure of electrochemically active carbons

Fig. 3 shows the obtained X-ray diffraction patterns for EAC1, EAC2, EAC3 and EAC4. The observed halos are typical of EAC2, EAC3 and EAC4. Moreover, the EAC3 and EAC4 patterns feature segments of a third halo in the 2Θ range from 10° to 15°. This is a characteristic structure for the latter two types of amorphous active carbons. Relatively high diffraction peaks appear in the X-ray diffraction pattern for EAC1, which evidence the presence of crystalline structures in this material.

An alternative explanation for the appearance of these peaks would be the incorporation of certain compounds left from the different production steps of the EAC1 material. It is worth noticing that the content of the crystalline product in EAC1 is fairly high and it is actually a component of the latter material.

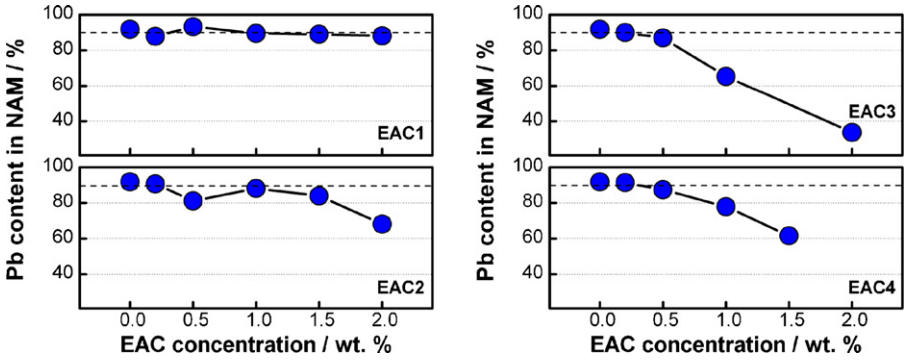

Fig. 4. Effect of EAC1–4 concentration on the degree of formation of the negative plates.

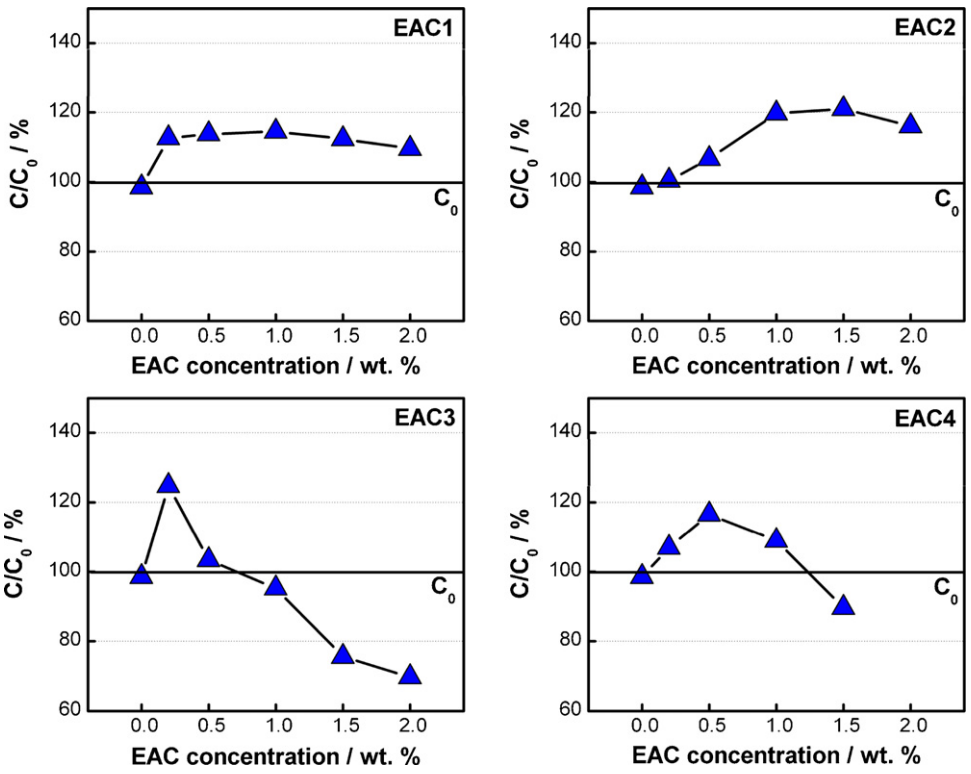

Fig. 5. C_{20} initial capacities for cells with EAC1–4 added to NAM versus EAC concentration.

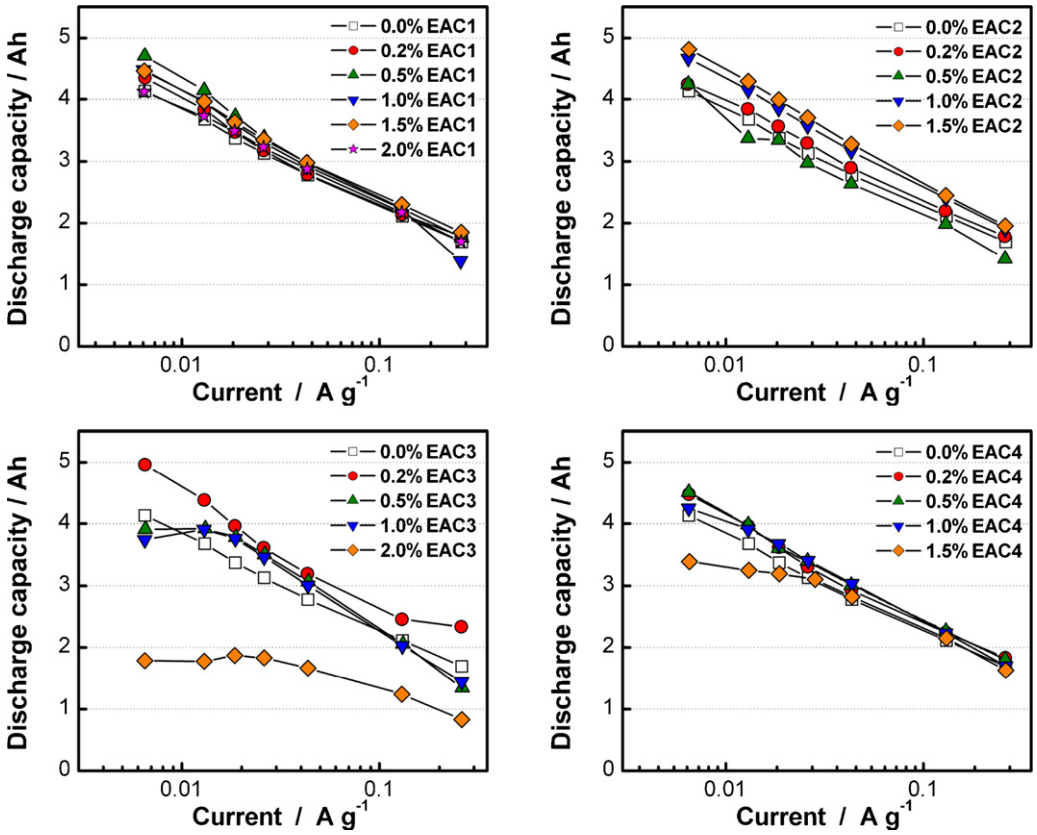

Fig. 6. Discharge capacity as a function of discharge current for cells with EAC1–4 additives at different concentration levels.

3.2. Performance of lead-acid cells with negative plates containing EAC additives

3.2.1. Efficiency of formation of the negative plates

As a first step to elucidating the effect of electrochemically active carbons on negative plate performance we estimated, by chemical analysis, the degree of formation of the negative plates with different carbon loads. Fig. 4 presents the obtained results in terms of Pb content in the negative active material after plate formation. It is accepted in battery technology that the negative plates are fully formed when the Pb content in NAM is higher than 90%.

The formation process is completed for the plates with EAC1 additive, irrespective of its concentration in NAM. Addition of EAC2, EAC3 or EAC4 to the negative paste, in concentration of 0.5 wt.%, does not affect the formation process. EAC3 and EAC4, at concentrations higher than 0.5 wt.%, decelerate the electrochemical processes of Pb formation. A new formation technology would be needed, supplying larger quantity of electricity, to complete the formation process. These results indicate that the type of electrochemically active carbon used influences the efficiency of NAM formation.

3.2.2. Initial capacity of the test cells

The initial performance tests comprised three C_{20} capacity measurements at 25 °C. Fig. 5 presents the obtained results from the third C_{20} capacity test for cells with different loads of EAC1–4 in NAM.

The cells with EAC1 or EAC2 at all concentration levels meet the standard requirement to deliver 100% of the rated capacity during the initial cycles. Initial capacity higher than the rated value have also cells with EAC3 at concentrations lower than 0.5 wt.% and EAC4 at concentrations lower than 1.0 wt.%. Cells with 1.0–2.0 wt.% EAC3 or 1.5 wt.% EAC4 are not completely formed. These cells need more than three initial cycles to reach the rated capacity value.

3.2.3. Peukert dependences for cells with EAC additives to NAM

The effect of carbons on the discharge performance of the cells at different current densities was evaluated based on the Peukert dependences. All cells obey the Peukert equation $I^n t = K$. The calculated values for n and K are in the range from −1.23 to −1.26 and from 0.038 to 0.049, respectively, depending on EAC concentration. Fig. 6 presents the dependences of cell capacity on discharge current for cells with EAC1–4 in NAM.

It is evident from the data in the figure that the discharge capacity is affected by the degree of formation of NAM with EAC3 or EAC2 additives. The capacity of cells with partially formed NAM decreases markedly, not only at low discharge currents. The greatest improvement in discharge capacity was observed with cells containing 1.0 wt.% or 1.5 wt.% EAC2, or 0.2 wt.% EAC3.

3.2.4. HRPSoC cycle life test. Influence of electrochemically active carbons on cell cycle life during the first cycle-set

A current profile simulating the micro-hybrid driving conditions is presented in Fig. 7a.

The changes in end-of-charge (Fig. 7b) and end-of-discharge voltages (Fig. 7c) during the above cycling test were used to evaluate the effect of EAC on the negative plate performance.

Fig. 8 summarizes the experimental data for the end-of-charge and end-of-discharge cell voltages during the HRPSoC test for cells with different levels of EAC1 included in NAM.

With increase of EAC1 concentration in NAM the end-of-charge voltage decreases from 2.56 V (at 0.2 wt.% EAC1) to 2.35 V (at 1.0 wt.% and 1.5 wt.% EAC1). Hence, increase of EAC1 load in NAM results in decrease of polarization of the negative plates during the charging step. The cycle life of the cell with 0.5 wt.% EAC1 in NAM is 11,300 HRPSoC cycles within the first cycle-set. This is the cell with the longest cycle life among all test cells with EAC materials added

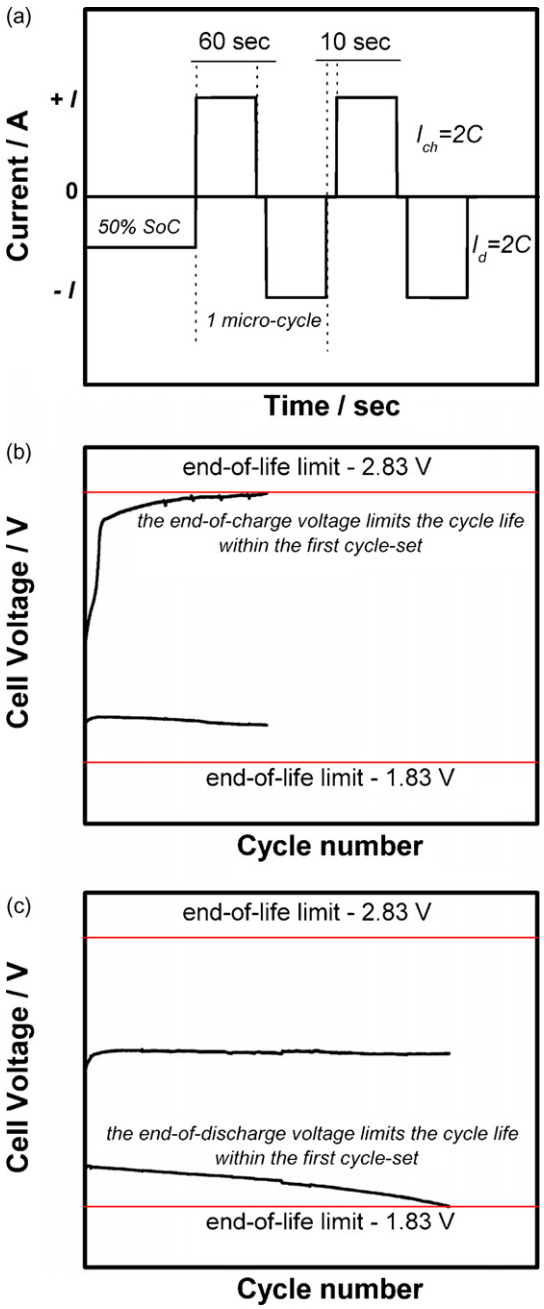

Fig. 7. (a) Current profile of a micro-hybrid driving test cycle; (b) end-of-charge voltage limits cell life within one cycle-set of the HRPSoC test; (c) end-of-discharge voltage limits cell life within one cycle-set of the HRPSoC test.

to NAM. The reference cell was highly polarized during charge. This cell performed only 1300 micro-cycles before reaching the upper voltage limit of 2.83 V.

The obtained cell voltage/cycle number curves for cells with EAC2, EAC3 or EAC4 are analogous to those presented in Fig. 8.

3.2.5. HRPSoC cycle life as a function of EAC content

The obtained results for the effect of EAC concentration on the cycle life (within the first cycle-set) of lead-acid cells operating under HRPSoC conditions are summarized in Fig. 9.

Cells with EAC1, EAC3 or EAC4 in NAM have the best cycle life performance, between 9200 and 11,600 cycles, at carbon concentration levels below or equal to 0.5 wt.%. On further increase of the EAC content, the cycle life of the cells decreases. Addition of EAC2

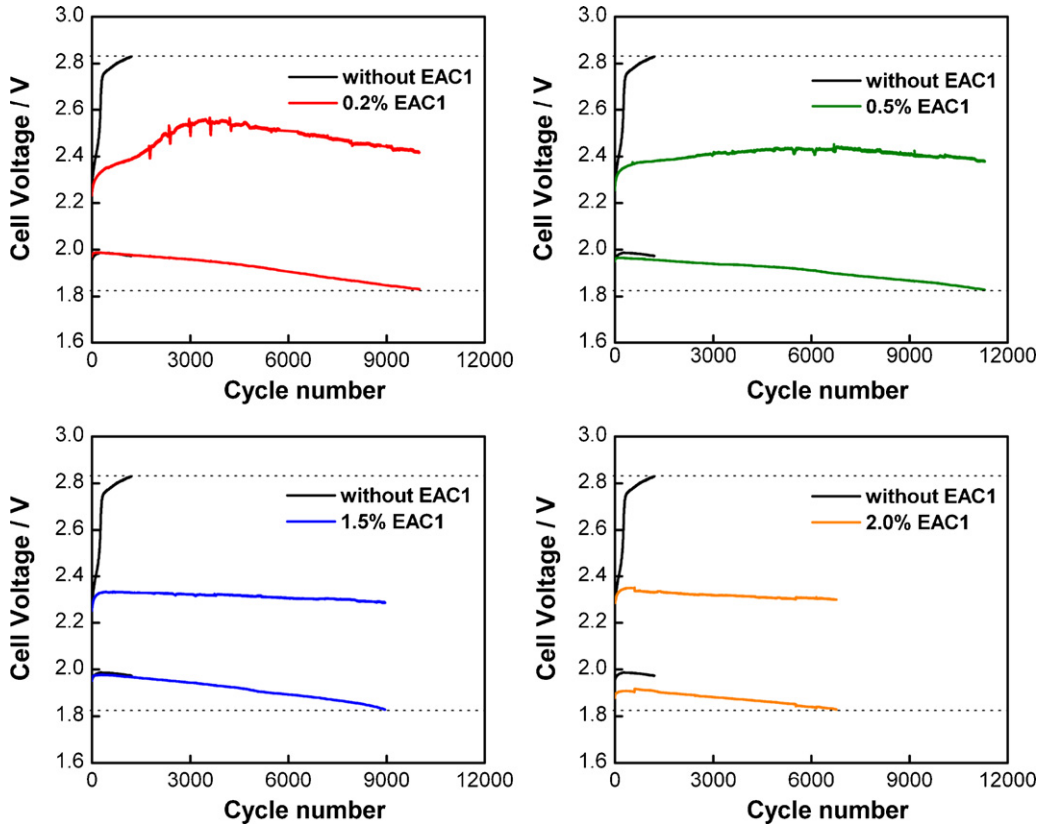

Fig. 8. End-of-charge and end-of-discharge cell voltages during the HRPSoC test for cells with different content of EAC1 in NAM.

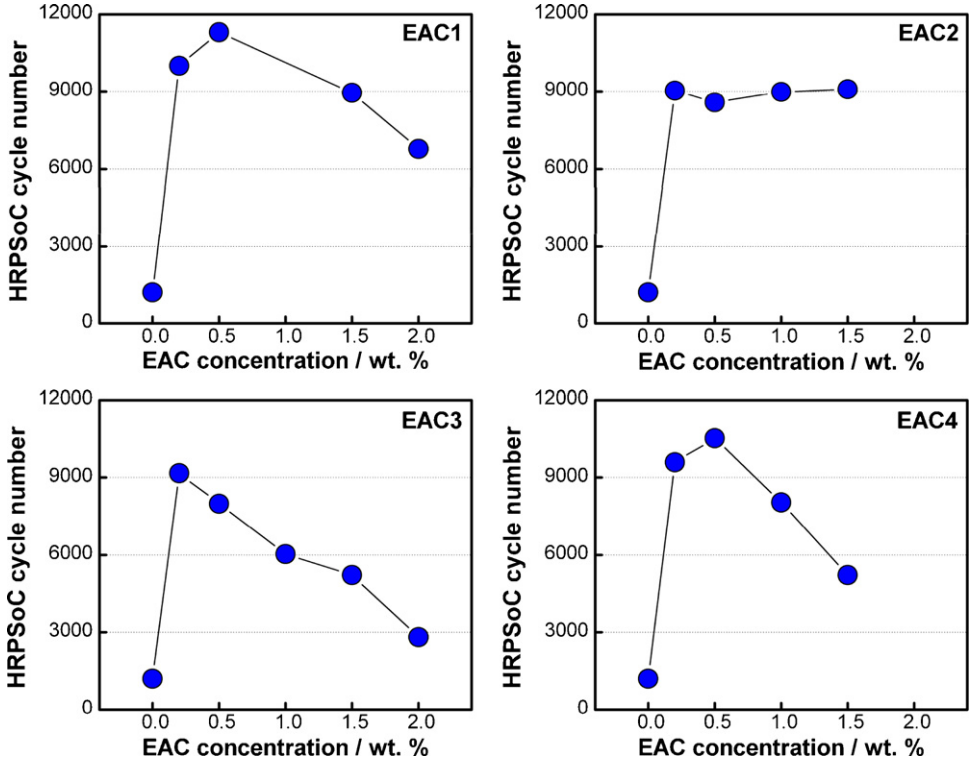

Fig. 9. HRPSoC cycle life (within the first cycle-set) as a function of EAC content in NAM.

to the negative paste in concentrations up to 1.5 wt.% results in cell cycle life of the order of 9000 cycles.

3.2.6. Teardown analysis of NAM after HRPSoC cycling

3.2.6.1. XRD and chemical analysis. Samples of the negative active material were subjected to teardown analysis in an attempt to elucidate how do electrochemically active carbons influence the cycle life of lead-acid cells under HRPSoC operation. Before the teardown analysis the cells were fully charged and then the physicochemical characteristics of NAM were examined by XRD, chemical analysis and SEM microscopy.

Fig. 10 presents the obtained XRD patterns for NAM samples (doped with EAC1–4) from the cells with the best cycle life performance during the first cycle-set. The results of the chemical analysis of the same samples are also included in the figures. No chemical analysis of the reference cell was performed.

The obtained results suggest that the state of charge of the cells was not sufficient to convert the accumulated $PbSO_4$ to Pb. Lead sulfate diffraction peaks are observed in all XRD patterns. Apart from $PbSO_4$, cells with 1.5 wt.% EAC2, 0.2 wt.% EAC3 or 0.5 wt.% EAC4 in NAM contain considerable amounts of α-PbO as well. Formation of α-PbO instead of $PbSO_4$ indicates that during cycling the electrolyte in the pores has become alkaline. The broad diffraction peaks of α-PbO are an indication of small crystallite size. The results of the chemical analysis of the samples are in good agreement with the XRD data, despite the fact that XRD detects only the crystal phases of NAM. The highest content of Pb is observed in the negative plate doped with 0.2 wt.% EAC3.

The obtained experimental results pose the following questions. Why is α-PbO phase formed in NAM during HRPSoC operation (Fig. 10)? Why is the cell voltage low during the HRPSoC cycling test (Fig. 8)? How do electrochemically active carbons contribute to the electrochemical reactions of charge of the negative plates? To answer these questions it is necessary to consider the influence of EAC on the structural and electrochemical characteristics of NAM.

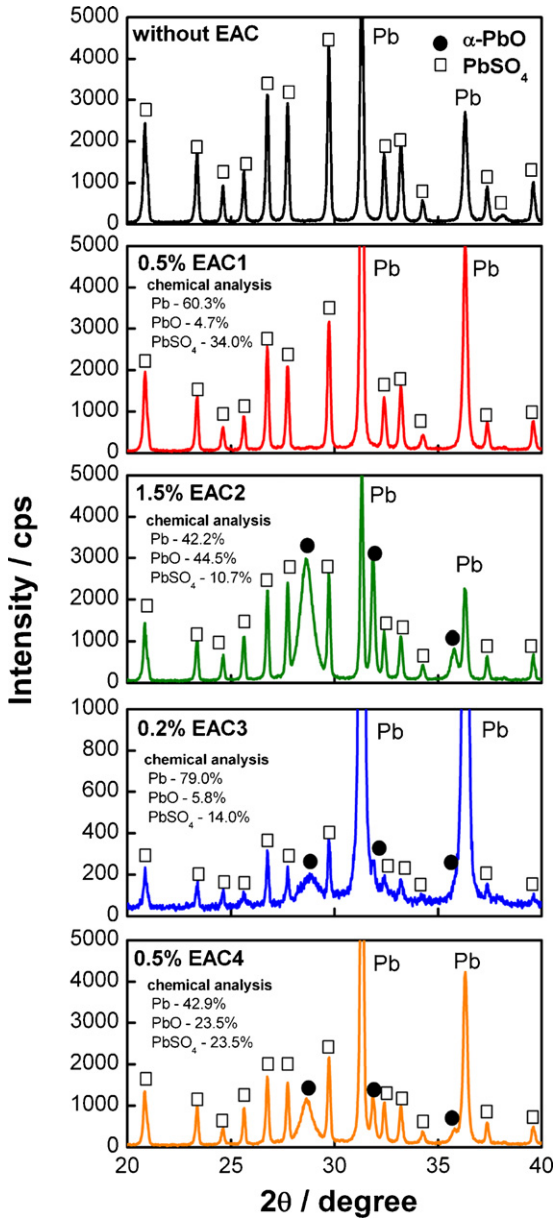

Fig. 10. XRD patterns for samples of NAM with EAC1–4 after the first cycle-set of the HRPSoC test.

3.3. Dynamics of the Pb + EAC interface of NAM during cycling

It was interesting to obtain information about the structure of NAM after the first cycle-set of the HRPSoC test. For the purpose, samples from the surface layer and from the interior of the negative plates were set to SEM examination. First, NAM samples were taken from the cells on completion of the first cycle-set (i.e. after they reached their end-of-life). Then the cells were re-charged to 100% SoC and new samples were taken for SEM examination.

Fig. 11 shows SEM images of NAM with 1.5 wt.% EAC2 in discharged state. It is evident that the surface layer of the negative plate (Fig. 11a and b) is highly sulfated and the NAM structure is partially destroyed. EAC2 particles (white spots) are adsorbed on the surface, or built in the structure, of the lead sulfate crystals thus causing formation of numerous defects in the $PbSO_4$ crystal structure and changing the shape of these crystals. These EAC2 particles lose their electrochemical properties because the contact between them and the Pb surface is interrupted.

The micrographs in Fig. 11c and d present SEM images of the interior of NAM with 1.5 wt.% EAC2. Because of the high charge and discharge currents employed during the HRPSoC test the charge and discharge reactions proceed mainly in the surface layers of the negative plates. Hence, only small amounts of lead sulfate are formed in the interior of the plates during discharge. It can be seen from the Fig. 11d that large surface area of Pb is covered by EAC2 particles. Lead sulfate crystals with well-shaped edges and apexes are also observed in the interior of the negative plate. These results indicate that crystal growth is mostly a result of recrystallization processes that occur in the inner parts of the negative plates.

Fig. 12a and b presents SEM images of the surface layers of NAM with 1.5 wt.% EAC2 in charged state.

During charge, the major part of the lead sulfate crystals dissolves. The released EAC2 particles are free to adsorb on new partially dissolved $PbSO_4$ crystals or on the Pb surface. These processes take place under the action of the ions and water diffusion flows.

SEM images of the inner parts of charged NAM with 1.5 wt.% EAC2 are presented in Fig. 12c and d. The Pb surface is covered by EAC2 carbon particles. Pb particles are organized mostly in the skeleton structure of NAM. The big lead sulfate crystals have partially dissolved and EAC2 particles have adsorbed on their surface.

On cycling of the cells, part of Pb is oxidized and $PbSO_4$ is formed during discharge and then the $PbSO_4$ crystals are reduced, partially or fully, to Pb on charge. Part of the carbon particles covering the Pb surface will desorb during discharge and then adsorb on the surface of $PbSO_4$ crystals. During charge, carbon particles will be involved in the reverse process. Consequently, the structure of NAM

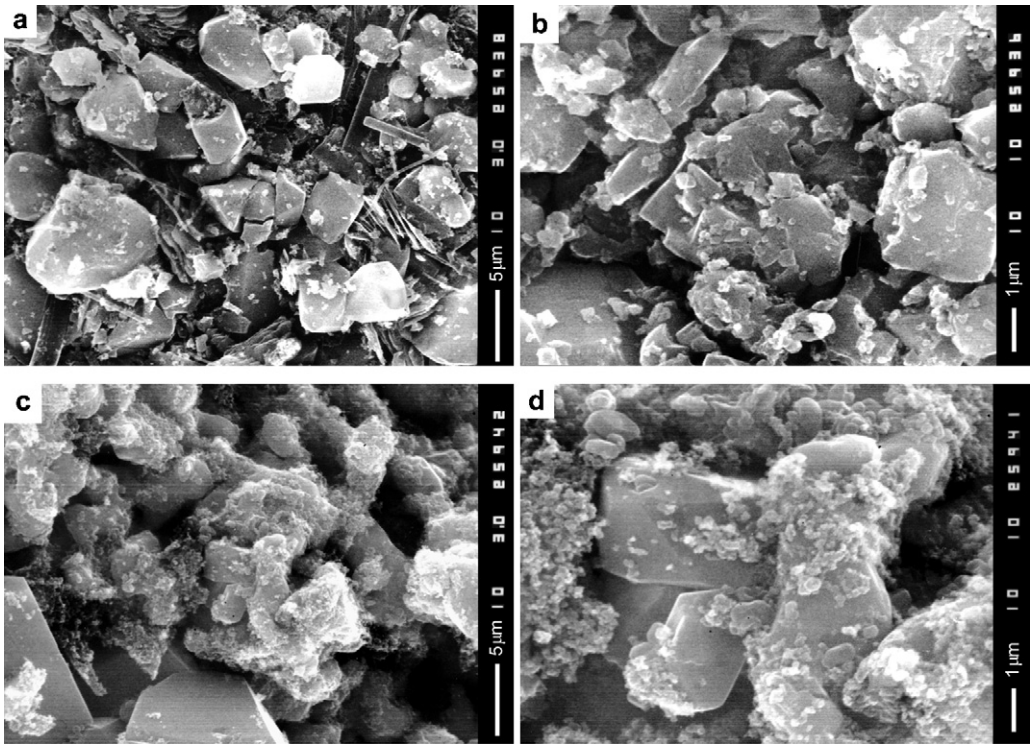

Fig. 11. SEM images of discharged NAM with 1.5 wt.% EAC2 after the first cycle-set of the HRPSoC test: (a) and (b) plate surface; (c) and (d) plate interior.

and of the interface NAM/solution will change during the cycling procedure and so will the number of carbon particles adsorbed on the Pb surface.

The above-presented SEM pictures (Figs. 11 and 12) evidence that, during cycling, the Pb + EAC interface of NAM structure undergoes continuous changes, i.e. a *dynamic state* is established in the Pb + EAC NAM structure.

The presence of two phases in the negative active mass: an electrochemically active one (Pb) and a second one (EAC) enhancing the electrochemical properties of the first one, raises the question about the optimal quantitative proportion between these two phases. Fig. 9 illustrates the effect of EAC type and content in NAM on the cycle life at HRPSoC conditions. The data in the figure indicate that there is a definite concentration range for each EAC type

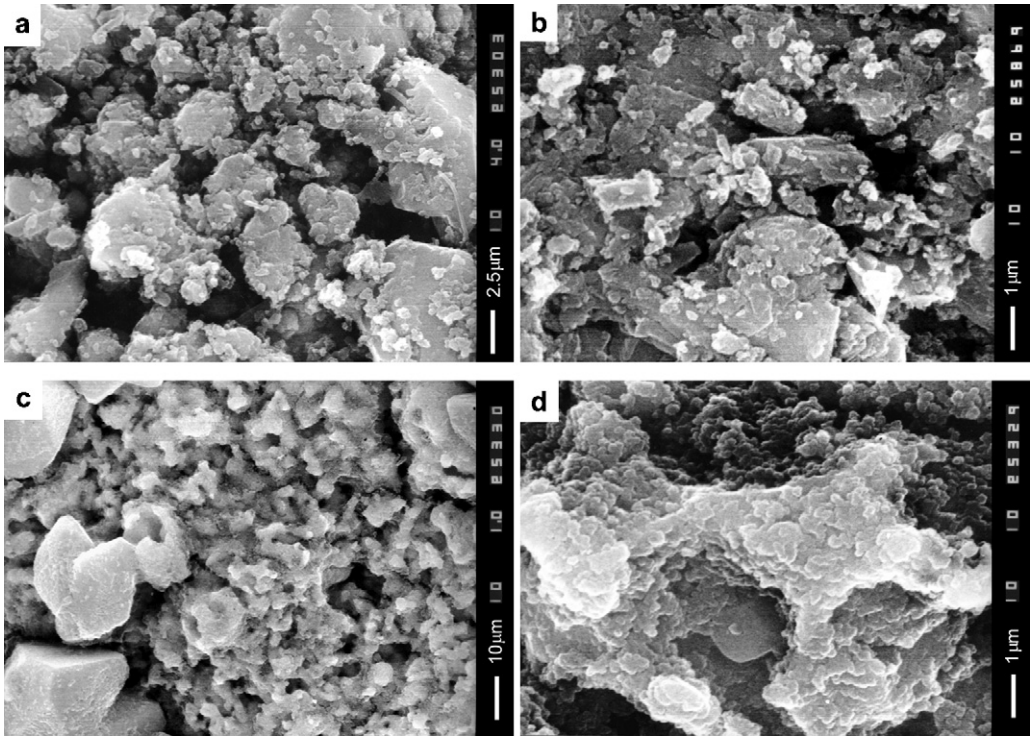

Fig. 12. SEM images of charged NAM with 1.5 wt.% EAC2 after the first cycle-set of the HRPSoC test: (a) and (b) plate surface; (c) and (d) plate interior.

which is able to ensure adequate battery cycle life as required for HEV applications.

3.4. Effect of EAC additives on the structural characteristics of NAM and on the electrochemical reactions

3.4.1. Pore volume distribution versus pore radius for NAM with EAC1–4 additives

Fig. 13 presents the differential pore volume distribution versus pore radius for formed NAM doped with EAC. The NAM samples were taken from the plates after formation.

The obtained results evidence that the pores of NAM without EAC additive have radii larger than 1.0 μm, most of the pore volume being distributed among pores with radii around 2.25 μm (median pore radius). Similar results are also obtained for NAM with addition of 0.5 wt.% EAC1 whose particles are bigger in size.

The porosity data for NAM with 1.5 wt.% EAC2, 0.2 wt.% EAC3 or 0.5 wt.% EAC4 are quite different. Judging by the pore volume distribution curves, negative active materials doped with these carbon additives have median pore radius below 1.0 μm. It can be concluded, then, that all four types of carbons under test change dramatically the pore system of the formed NAM by reducing strongly its pore radius.

Fig. 13 summarizes also the total pore volume values obtained for the above-mentioned NAM samples. The lowest total pore volume is measured for NAM without EAC dopants. Addition of EAC to the negative paste results in increase of the total pore volume of NAM. The most noticeable effect is observed with EAC1 when added in concentration of 0.5 wt.%.

Thus, EAC additives significantly alter the structure of NAM by increasing its total pore volume and decreasing its mean pore radius.

3.4.2. Median pore radius of NAM with EAC1–4 additives

The dependences of median pore radius of NAM on amount of added carbons, as determined from the porograms, are plotted in Fig. 14.

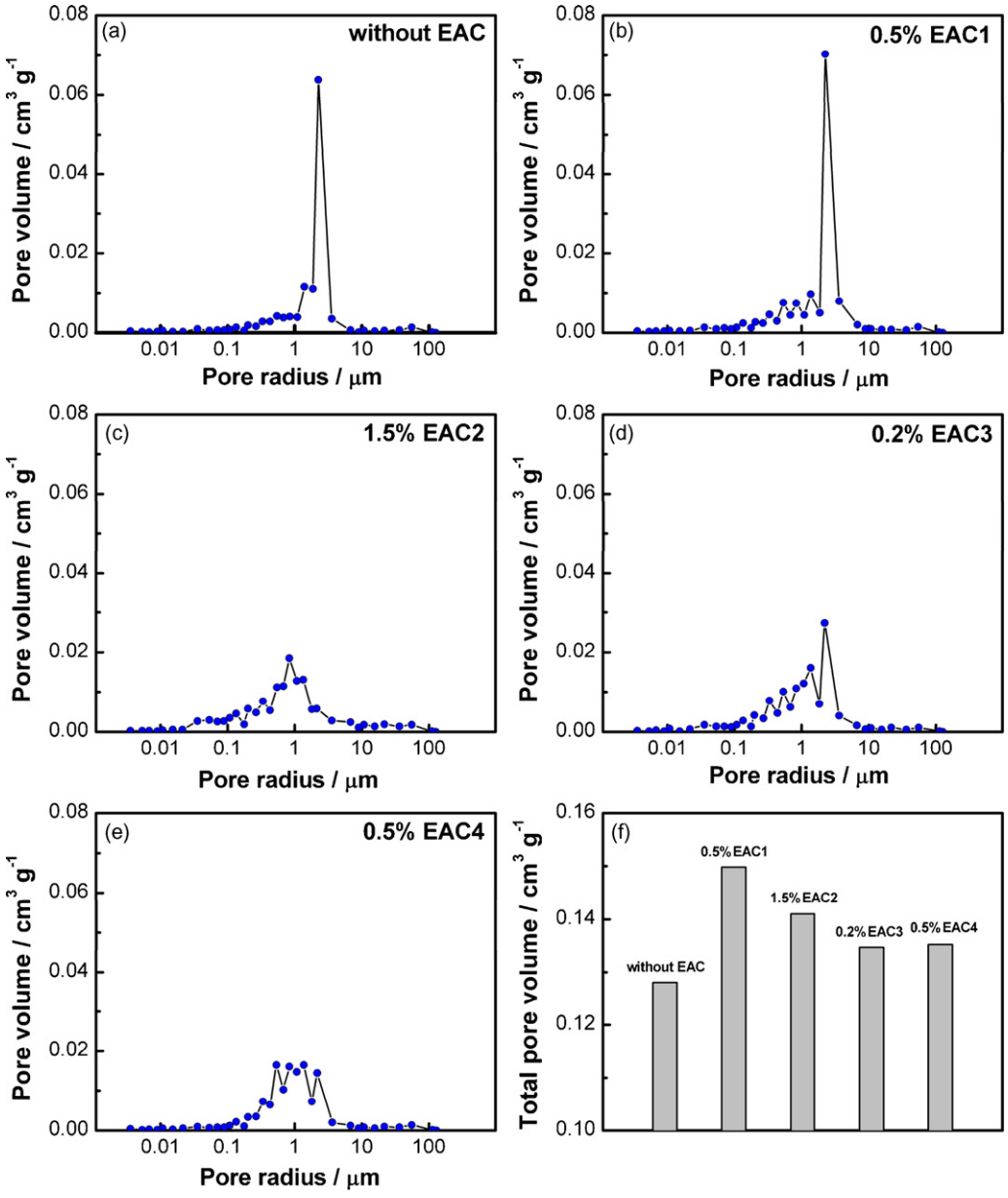

Fig. 13. Pore volume distribution versus pore radius of formed NAM: (a) without EAC; (b–e) with EAC1–4 additives; (f) total pore volume of formed NAM with different loads of EAC1–4 additives.

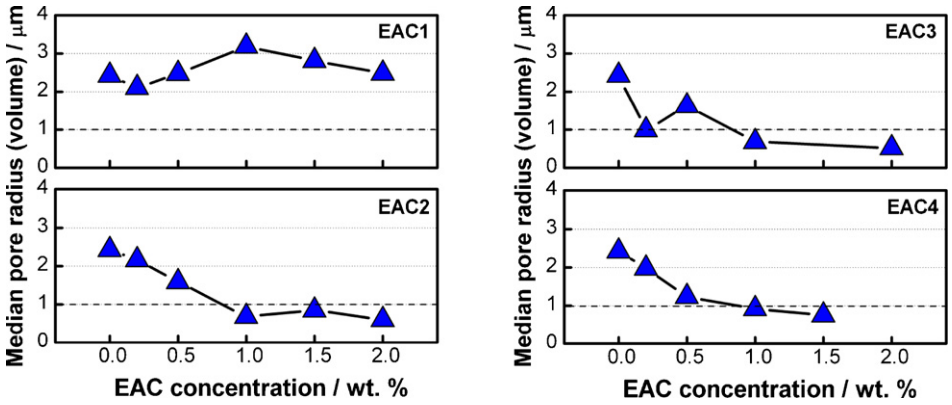

Fig. 14. Median pore radius of NAM versus EAC1–4 carbon concentration.

For all studied concentrations of EAC1 in NAM the mean pore radius is within the range 2–3 μm. Additions of EAC2, EAC3 or EAC4 to NAM reduce the median pore radius and it may drop below 1 μm at EAC loads higher than 1.0 wt.%. At concentrations of EAC2, EAC3 or EAC4 close to 2.0 wt.%, the median pore radius decreases to 0.5 μm. Through this influence of carbon additives on the pore system of NAM they will reduce the rate of the ionic fluxes in the inner parts of the plate and subsequently change the electrochemical and chemical reactions that proceed at the negative plates.

3.4.3. Correlation between HRPSoC cycle life of lead-acid cells with EAC additives and median pore radius of NAM

Fig. 15 presents the dependences HEV cycle life versus mean pore radius of NAM for test cells with the four types of EAC additives.

The following conclusions can be drawn on grounds of the data in the figure:

(a) The best cycle life performance within the first cycle-set of the simulated HRPSoC test is registered with the cells with EAC2, EAC3 or EAC4 additives which yield NAM with mean pore radius within the range from 0.7 μm to 2.0 μm. As evidenced by Fig. 2, these EAC particles are spheroid in shape, but have different radii. The cells with addition of EAC1, have the longest cycle life at NAM mean pore radius of between 2.0 μm and 2.7 μm.
(b) As indicated by the XRD data (Fig. 10), on HRPSoC cycling of cells containing EAC2, EAC3 or EAC4 in NAM, α-PbO is formed in the NAM beside $PbSO_4$. The mean pore radius of these negative active masses is less than 1.5 μm. No α-PbO forms in the NAM of plates with EAC1, where the mean pore radius is 2.5 μm. This implies that *movement of the H_2SO_4 flows in the NAM with mean pore radius smaller than 1.5 μm is strongly impeded. Hence, the solution in the pores is alkalized, which results in formation of α-PbO*. Indeed, the highest amount of α-PbO is detected in the NAM with 1.5 wt.% EAC2, which has the smallest mean pore radius of 0.7 μm. Thus, through their influence on the mean pore radius of NAM, electrochemically active carbons can influence also the mechanism of the overall electrochemical reaction of charge and discharge of the negative plates, and can change it to $Pb \rightleftharpoons Pb(OH)_2 \rightleftharpoons$ α-PbO.

3.5. Influence of EAC on the elementary processes involved in the electrochemical reaction of charge of lead-acid battery negative plates

3.5.1. BET surface area of NAM with EAC1–4 additives

The relationship between BET surface area of NAM and amount of added carbons is presented in Fig. 16.

Depending on the type of activated carbon used, addition of EAC can change the surface area of NAM from 0.9 $m^2\,g^{-1}$ (EAC2) to 20 $m^2\,g^{-1}$ (EAC3). These results indicate that the specific surface of NAM is determined not only by the specific surface of lead (which is 0.49 $m^2\,g^{-1}$) but also by the specific surface of the additive, which is 6 times higher than that of lead for EAC2 and 42 times higher for NAM with EAC3, respectively. The highest specific BET surface area value was obtained for the NAM with 2.0 wt.% EAC3 added to the paste.

3.5.2. Correlation between HRPSoC cycle life of lead-acid cells with EAC additives to NAM and BET surface area of NAM

The processes of charge and discharge of the negative plates proceed at the interface Pb/electrolyte solution in the pores of NAM. EAC particles are electronic conductors. Adsorbed on the Pb surface, EAC particles create a new electrochemically active interface: EAC/electrolyte having the potential of the Pb/electrolyte interface. Probably, electrochemical reactions proceed at this interface, too.

In an attempt to investigate the influence of EAC on the electrochemical reactions at the negative plates we studied the correlation between cell cycle life and BET surface area of NAM.

Fig. 17 presents the HRPSoC cycle life of the test cells versus the specific BET surface area of NAM. The EAC weight percent concentrations in NAM are also given in the figure.

The experimental data presented in Fig. 17 give grounds for the following conclusions:

(a) *The different EAC additives have different effect* on the dependence HEV cycle number versus NAM BET surface. The best cycle life performance (>9000 cycles) is observed with the cells with NAM specific surface area of up to 4 $m^2\,g^{-1}$. Such surface values are measured for NAM with addition of EAC1 or EAC4 in concentrations of up to 0.5 wt.%. Knowing that the specific surface of Pb is 0.5 $m^2\,g^{-1}$, it follows that the ratio EAC:Pb surface should be maximum 7:1. On further increase of the specific surface of NAM, the cycle life of the cells in HRPSoC regime declines.
(b) *Behaviour of cells with specific NAM surface lower than 4 $m^2\,g^{-1}$*. With increase of the specific surface of NAM from 0.5 $m^2\,g^{-1}$ to 4 $m^2\,g^{-1}$, the curves HEV cycles/NAM surface pass through a maximum, S_{max} (for cells with EAC1 or EAC4).
(c) *Behaviour of cells with specific NAM surface area higher than 4 $m^2\,g^{-1}$*. The data in Fig. 17 indicate that with increase of the NAM surface area above 4 $m^2\,g^{-1}$, through increase of the EAC content in NAM, the life of the cells declines. The slope of this decline depends on the type of additive used. Thus, for example, the cycle life of cells with EAC4 additive decreases more quickly

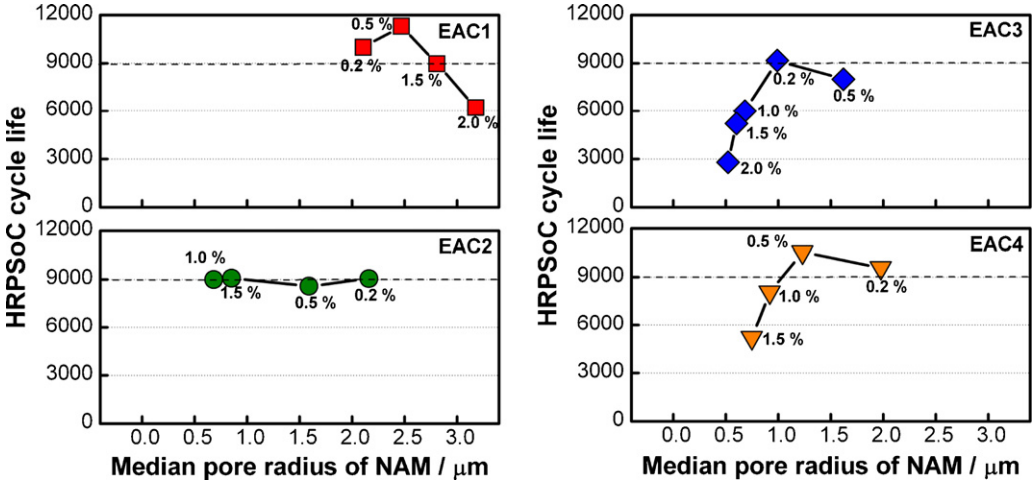

Fig. 15. HRPSoC cycle life of the test cells versus median pore radius of NAM doped with EAC1–4.

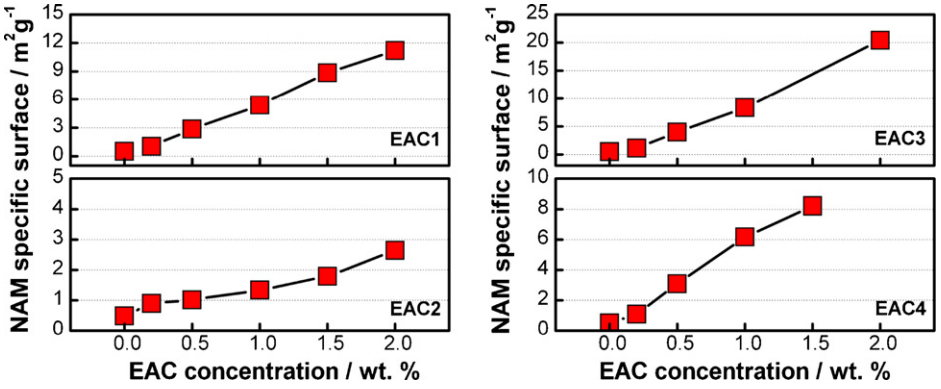

Fig. 16. BET surface area of NAM doped with EAC1–4 as a function of carbon concentration.

with increase of NAM surface than in the case of cells with EAC3 additive.

The cell cycle life depends on the surface of NAM and the latter is formed mostly by the surface of EAC particles. Hence, the electrochemical reactions will proceed not only on the Pb surface, but also on the surface of the EAC phase. The EAC interface contributes to the transfer of electrons to Pb^{2+} ions, and to the formation of Pb atoms. So reduction of $PbSO_4$ proceeds on the EAC surface as well.

3.5.3. *Microstructure of NAM with EAC2 or EAC4 additives after formation*

Since the electrochemical processes take place at the interface of NAM with the solution the coverage of NAM by carbon particles will play crucial role in the capacity and cycle life performance of the negative plates. Fig. 18 presents SEM micrographs of formed NAM containing different concentrations of EAC4.

The images illustrate the coverage of the Pb surface by EAC4 particles. They are adsorbed on the lead surface. With increase of EAC4 concentration in NAM, the Pb surface coverage by EAC4

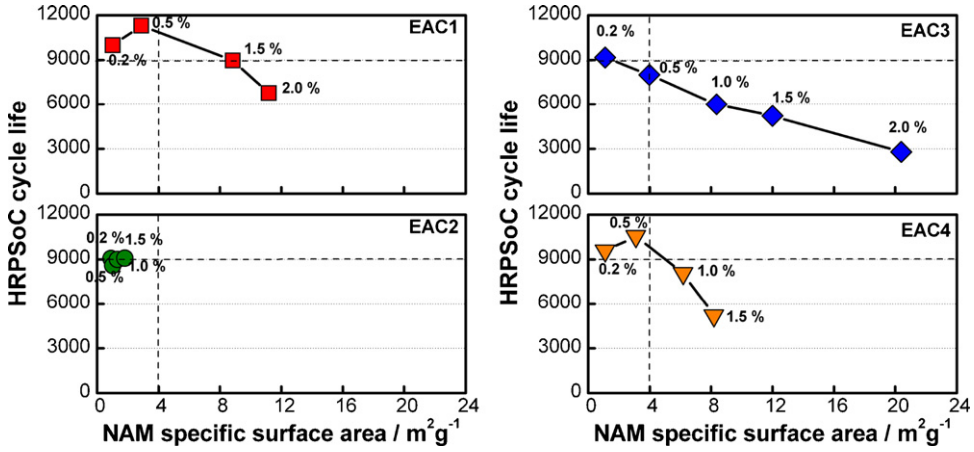

Fig. 17. HRPSoC cycle life of the test cells versus NAM specific surface area.

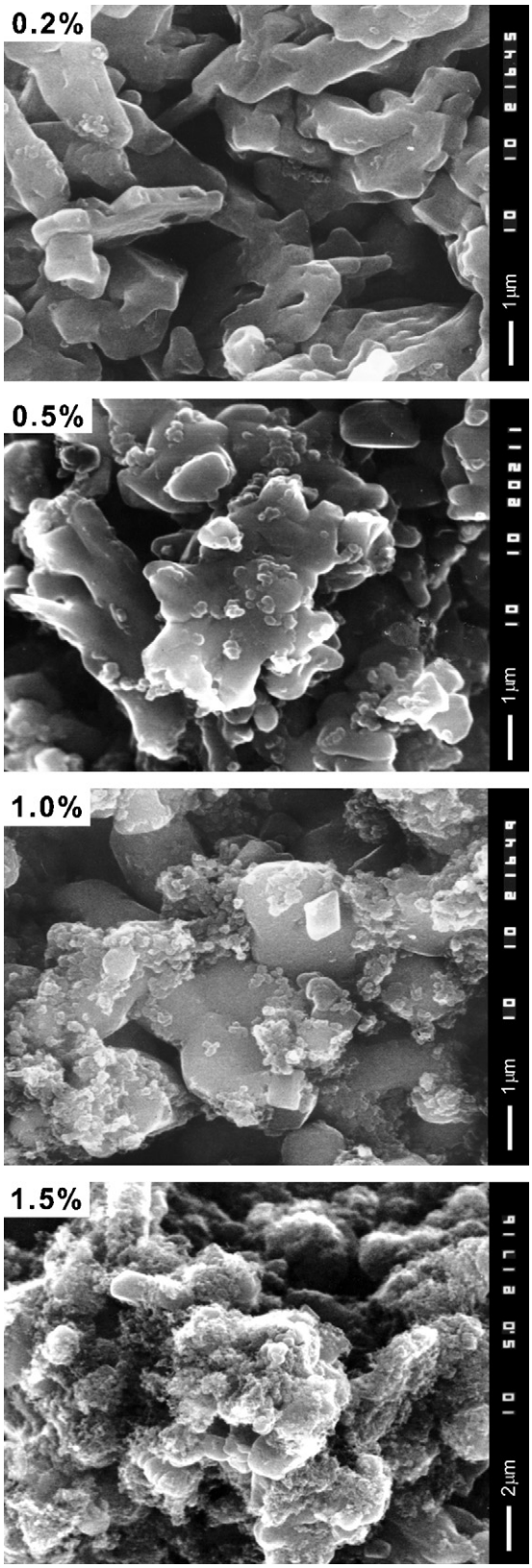

Fig. 18. Crystal morphology of NAM doped with different concentrations of EAC4.

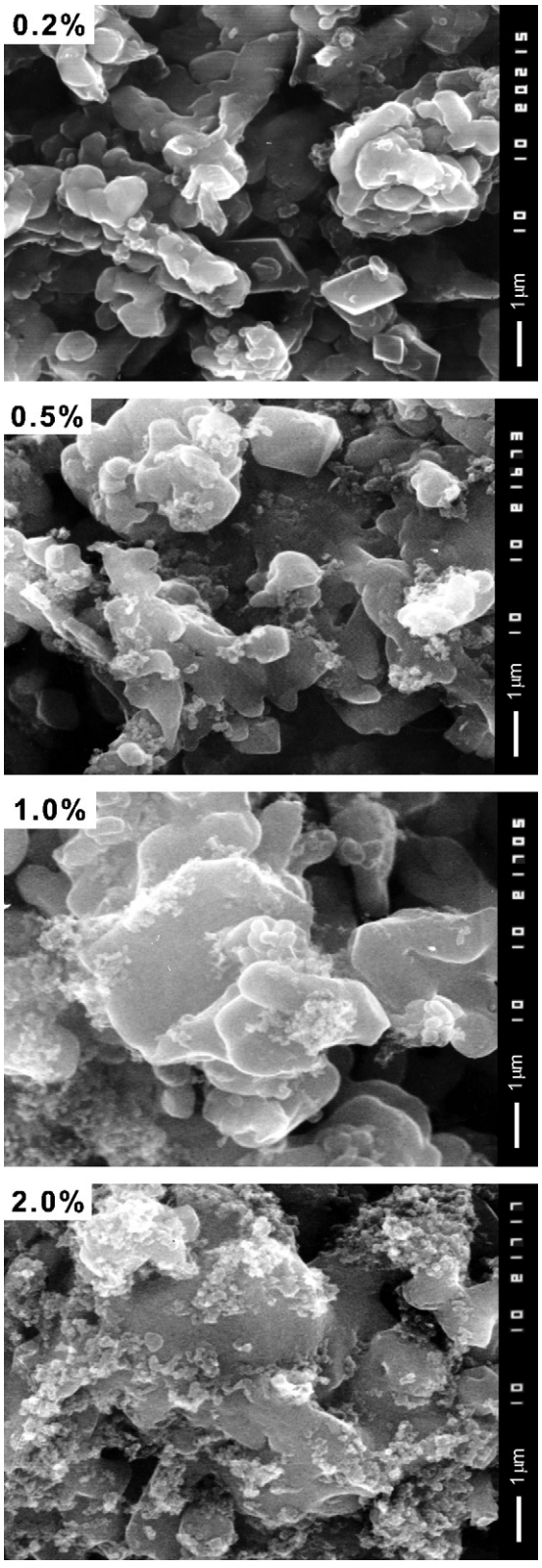

Fig. 19. SEM images of the structure of NAM with different loads of EAC2.

particles increases rapidly and the free Pb surface decreases. At 1.5 wt.% EAC load, the Pb surface is almost completely covered by EAC particles. The specific surface area of NAM becomes larger than $4\ m^2\ g^{-1}$.

This is not the case with NAM doped with EAC2 (Fig. 19). As evident from the SEM pictures in Fig. 19, when added in concentrations of 0.2 wt.% or 0.5 wt.%, EAC2 carbon particles are randomly distributed on the Pb surface. At higher EAC2 levels the lead surface is partially covered by EAC and even at

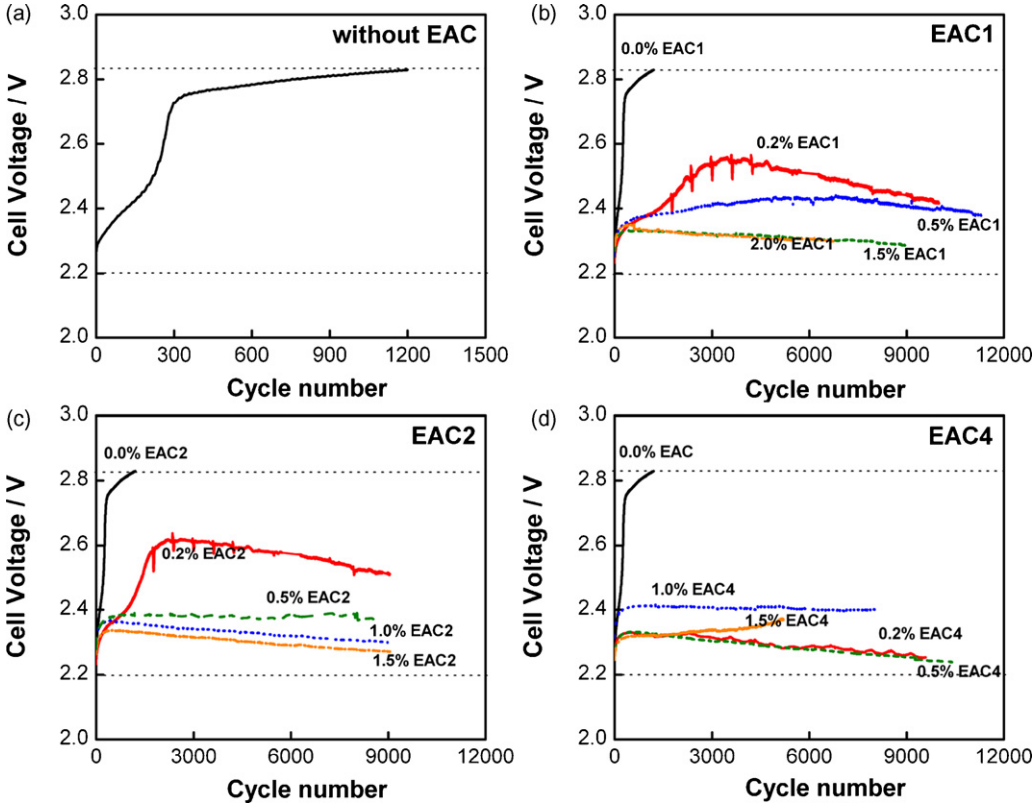

Fig. 20. End-of-charge-voltage versus HEV cycle number for cells with different concentrations of carbon additives in NAM: (a) without EAC additive; (b) with EAC1; (c) with EAC2; (d) with EAC4.

2.0 wt.% EAC2 content in NAM, large areas of Pb remain free from EAC2 particles. The specific surface area of NAM is lower than $4\,m^2\,g^{-1}$.

3.6. Parallel mechanism of the charge processes at the negative plates containing EAC additives

3.6.1. Elementary processes which limit the charging rate of the negative plates

As described in Section 2 of this paper, the test cells comprised 3 positive and 2 negative plates, i.e. the positive plates were oversized (0.5 mm thicker) as compared to the negatives, thus their potential would change but very slightly during cycling. So it can be assumed that the changes in cell voltage on cycling are due to changes of the potential of the negative plates.

Another indication of the involvement of the EAC surface in the electrochemical reactions is the relationship end-of-charge cell voltage versus cycle number for all cells under test. The obtained dependences are presented in Fig. 20.

Polarization of the reference cell with no EAC in NAM increases by 400 mV within the first 300 cycles already. This indicates that the electrochemical reaction of Pb^{2+} reduction on the Pb surface is very much impeded. The short cycle life of this cell implies that $PbSO_4$ has accumulated rapidly during the charge/discharge processes leading to considerable cell polarization and hence shortening of its life to only 1300 HEV cycles.

Polarization of the cells with EAC1, EAC2 or EAC4 depends on the concentration of the EAC added to NAM and is less than 100 mV for EAC1 containing cells, and 50 mV for the cells with EAC2 or with low concentrations of EAC4. Similar behaviour is also observed with the cells with addition of EAC3 to NAM.

If EAC additives reduce the polarization of the negative plates, then obviously they will accelerate the charge processes. Let us see which elementary processes can be accelerated by carbon additives.

(a) *Reversible and irreversible processes of $PbSO_4$ formation and dissolution.* In the HRPSoC cycling mode, discharge is conducted at fairly high currents (2*C* A). This results in high oversaturation of the solution in the NAM pores with Pb^{2+} ions [10]. These ions form small $PbSO_4$ crystallites (nuclei). The latter are highly soluble and will maintain a high concentration of Pb^{2+} ions in the pore solution (Ostwald–Freundlich equation). The elementary process of $PbSO_4$ dissolution on HRPSoC cycling will proceed at a high rate and hence will not impede the charge process (Fig. 21).

However, not all Pb^{2+} ions formed during the charge cycle produce small readily soluble $PbSO_4$ crystallites. Some of the ions are incorporated in the lead sulfate crystals already formed. These crystals grow and become difficult to dissolve, thus part of the Pb^{2+} ions are excluded from the reversible charge/discharge cycle. Sulfation of the plates proceeds at a low rate but, after a certain number of cycles, ample amount of lead sulfate accumulates, which leads to end-of-life of the cells.

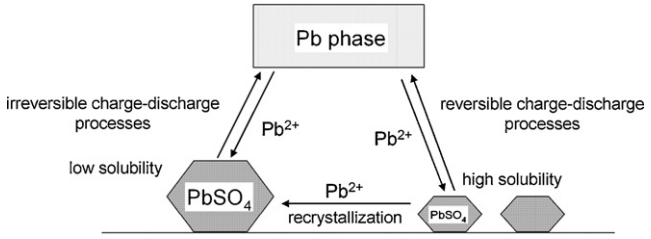

Fig. 21. Diagrammatic representation of the reversible and irreversible charge/discharge processes during polarization of the negative plates.

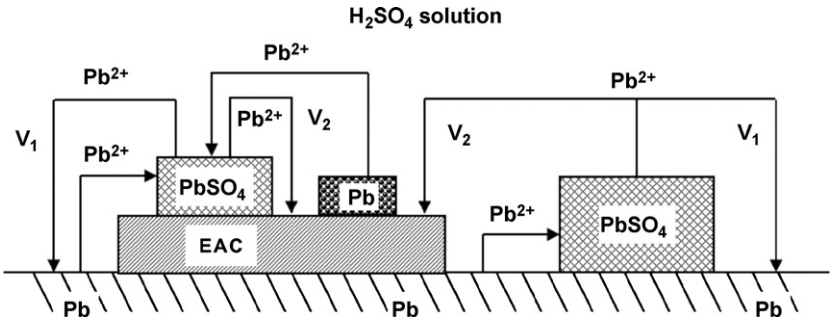

Fig. 22. Schematic representation of the parallel mechanism of charge of the negative plate. The reaction of Pb^{2+} reduction proceeds on both the Pb and EAC surfaces.

So during HRPSoC cycling two types of processes take place simultaneously at the negative plates: *reversible processes* yielding small $PbSO_4$ crystallites which dissolve easily and thus maintain high charging rate, and *irreversible processes* during which Pb^{2+} ions contribute to the growth of big $PbSO_4$ crystals of low solubility, which accumulate progressively and lead to sulfation of the plates. The ratio between these two types of processes determines the cycle life of the cells on HRPSoC operation. Electrochemically active carbon additives change this ratio in favour of the reversible processes and thus improve the cycle life performance. So the reason for the observed retarded charge of negative plates with no carbon additives should be looked for in the subsequent elementary processes of charge.

(b) *Diffusion of Pb^{2+} ions in the NAM pores*. This process will also proceed at a high rate, because of the high Pb^{2+} concentration gradients created in the pore solution on HRPSoC cycling. So Pb^{2+} ion diffusion, too, will not impede the charge process despite the short charge/discharge cycles with high currents. This leaves the remaining two elementary processes of charge to be held responsible for the retarded charge process.

(c) *Charge transfer and reduction of Pb^{2+} ions*. During charge of the negative plates, the double electric layer of the interfaces Pb/solution and EAC/solution is charged and, when the potential reaches a definite value, electrons transfer from the metal surface to the adsorbed Pb^{2+} ions and the reaction $Pb^{2+} + 2e^- \rightarrow Pb$ proceeds. The potential at which electrons will overcome the potential barrier of the interface depends on the nature of the interface and on its structure. Comparing the cell voltage curves for the cells with EAC and for the reference cell with no carbon additive (Fig. 20) it can be seen that the potential at which the reduction of Pb^{2+} ions proceeds on the EAC surface is much lower than that of the same electrochemical reaction on the Pb surface. This means that the potential barrier that electrons have to overcome at the EAC/solution interface is much lower than at the Pb/solution interface. Hence, the electrochemical reaction of Pb^{2+} reduction proceeds predominantly on the EAC surface. The potential at which this reaction proceeds will depend on the concentration of the carbon additives in NAM.

(d) *Formation of Pb phase*. The data in Fig. 20 evidence that with increase of the content of EAC1 or EAC2 in NAM the overpotential of reduction of Pb^{2+} ions decreases. The only exception from this tendency is the cell with EAC4, where higher additive concentrations yield higher electrode potential. Probably, in this case Pb nucleation and crystal growth proceeds with less hindrances on the Pb surface than on the surface of EAC particles. Lead atoms tend to be incorporated in Pb growth fronts more easily than to form new nuclei on the surface of foreign substrates. The SEM pictures in Fig. 18 show that at high EAC4 concentrations there is but very small free lead surface and hence Pb atoms have to form a new phase on the EAC surface. This would slow down the electrochemical reaction and would increase slightly the charging potential of the negative plates, which is actually observed in Fig. 20.

So electron transfer during the electrochemical reaction of Pb^{2+} reduction proceeds at much lower potentials at the EAC/solution interface than at the Pb/solution interface. The subsequent elementary process of incorporation of Pb atoms in the Pb growth fronts will proceed much easier than the formation of a new phase on the EAC surface. The obtained Pb atoms may, by surface diffusion, reach the Pb surface and be incorporated into the latter's structure, or they may form Pb nuclei on the surface of EAC particles, thus reducing the EAC surface area on which the reduction of Pb^{2+} ions proceeds.

Thus, electrode polarization will depend on the ratio between the EAC and Pb surfaces. This correlation is supported by the experimental results presented in Fig. 17. The best cycle life performance is registered for the cells with EAC:Pb surface ratio equal to 7:1 and NAM specific surface area of 4.0 $m^2\ g^{-1}$. When the specific surface of NAM is above this value, the lead surface

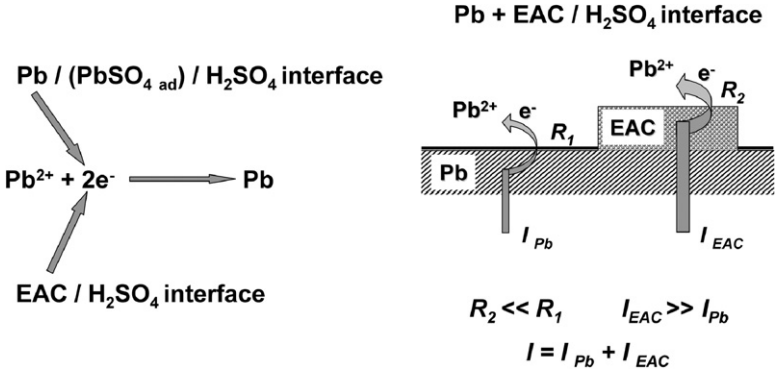

Fig. 23. Schematic representation of the charge transfer through the (Pb + EAC)/H_2SO_4 interface in NAM.

diminishes, which reduces substantially the reversibility of the processes in the cell and hence its cycle life is shortened.

Based on the obtained experimental results it can be concluded that addition of electrochemically active carbons to the negative active material improves the reversibility of the charge/discharge processes on the lead sulfate electrode by creating a "*parallel mechanism of the charge reactions*".

3.6.2. A model for the parallel mechanism of charge

Fig. 22 shows a schematic diagram of the charge and discharge processes that take place on negative plates with NAM containing EAC additives.

During discharge, the following electrochemical reaction proceeds on the lead surface:

$$Pb \rightarrow Pb^{2+} + 2e^{-}$$

Pb^{2+} ions diffuse to the nearest $PbSO_4$ crystal and precipitate on its surface, thus contributing to its growth. $PbSO_4$ crystals grow on the surface of both Pb and EAC particles (Figs. 11 and 12). The concentration of Pb^{2+} ions in the solution is determined by the solubility product of $PbSO_4$. During charge, the Pb^{2+} ions from the solution are reduced on the Pb surface at a rate V_1 and on the EAC surface at a rate V_2. When an electrochemical reaction proceeds simultaneously on two surfaces of different nature, the electrode potential is determined by the reaction with the higher rate. The polarization of the negative electrode is determined by the rate V_2, as shown in Fig. 20.

Fig. 23 presents a schematic diagram of the electric charge transfer through the (Pb + EAC)/H_2SO_4 interface.

Besides the layer of expander molecules, a monolayer of adsorbed $PbSO_4$ molecules forms on the lead surface due to the high acid concentration there. The charge transfer resistance of these adsorbed layers of the Pb/H_2SO_4 interface is high. No such barrier layers are formed at the EAC/H_2SO_4 interface and the electron transfer through this interface proceeds with less resistance. The electric current that flows through the EAC/H_2SO_4 interface is much higher than that flowing through the Pb/H_2SO_4 one. So, the adsorbed EAC particles on the Pb surface play the role of by-pass for the electron transfer and thus accelerate the electrochemical reaction of Pb^{2+} ion reduction. Thus, carbon added to the negative plate acts as electrocatalyst to the charge reaction.

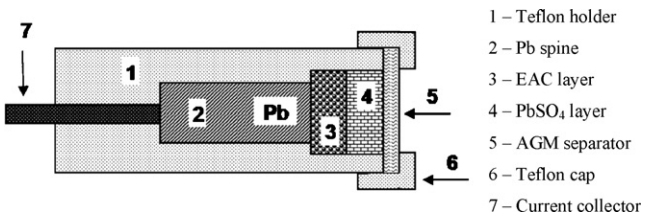

Fig. 24. Multi-layer model electrode design.

3.6.3. Experimental verification of the parallel mechanism of charge of negative plates with electrochemically active carbons

The proposed parallel mechanism of charge was verified experimentally using a model electrode (ME) analogous to the one used in an earlier investigation of ours [11]. The modified design of the model electrode is presented diagrammatically in Fig. 24.

The base of the Pb–0.1%Ca spine, inserted in PTFE holder, was covered with one or two layers of different materials, thus forming three different electrodes as follows:

- A layer of chemically prepared $PbSO_4$. This ME modification, referred to as Pb/$PbSO_4$ electrode, was used to measure the current of $PbSO_4$ reduction on the Pb surface.
- A layer of electrochemically active carbon. This ME, referred to as Pb/EAC electrode, was used to investigate the processes on polarization of the EAC layer in H_2SO_4 solution.
- Both EAC and lead sulfate layers, referred to as Pb/EAC/$PbSO_4$ electrode and used to study the processes of $PbSO_4$ reduction on the EAC surface.

A sheet of AGM separator was placed over the investigated layers then pressed with a PTFE cap. This electrode design confines trans-

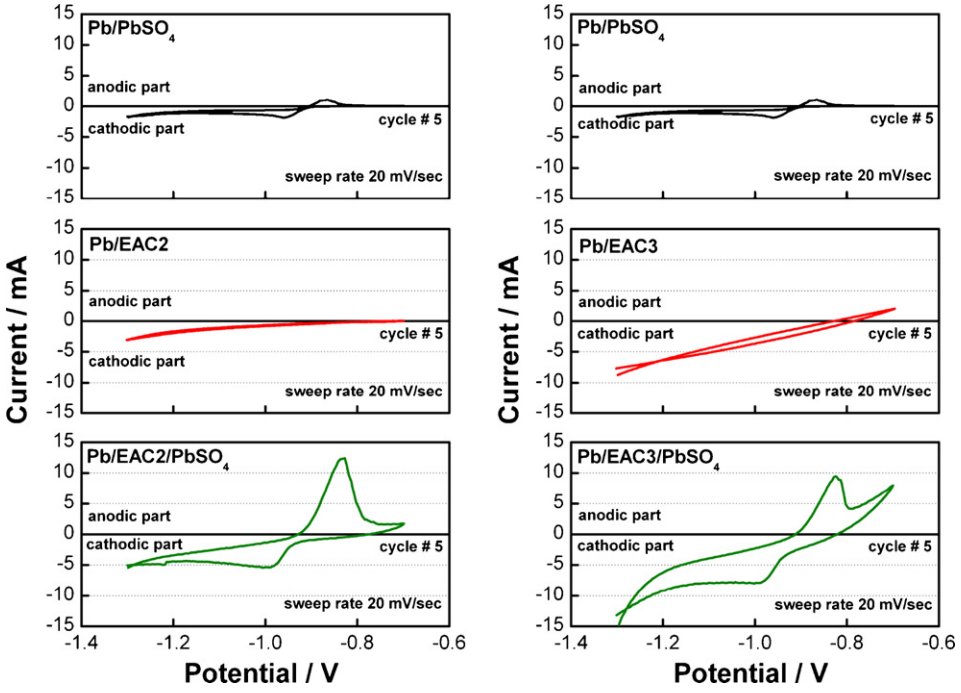

Fig. 25. Voltammograms for the three types of model electrodes (Pb/$PbSO_4$, Pb/EAC and Pb/EAC/$PbSO_4$) with EAC2 or EAC3 carbon layer.

fer of materials from the ME to the electrolyte. The experiments were carried out in a classical three-electrode cell comprising a ME as working electrode, an $Hg/HgSO_4/H_2SO_4$ reference electrode and a large Pt mesh as counter electrode. All experiments were performed in excess of 1.28 sp.gr. sulfuric acid solution at ambient temperature. Linear sweep voltammetry measurements were conducted. The potential of the working electrode was swept between −0.7 V and −1.3 V at a scan rate of 20 mV s^{-1}.

Fig. 25 presents the obtained voltammograms, at the 5th polarization run, for the three types of model electrodes with EAC2 or EAC3 additives.

- *$Pb/PbSO_4$ electrode*. The curve profile is similar in shape to that of the voltammogram for $Pb/PbSO_4$ electrode immersed in H_2SO_4 solution. The current is low due to the small free lead surface that is contact with the electrolyte solution.
- *Pb/EAC electrode*. The obtained voltammogram resembles that of a double layer capacitor. The double layer of the interface is charged and discharged and no Faraday reaction proceeds at that.
- *$Pb/EAC/PbSO_4$ electrode*. The $PbSO_4$ layer sustains a certain concentration of Pb^{2+} ions in the solution filling the pores of the $PbSO_4$ and of the EAC layers, which is determined by the solubility of $PbSO_4$.

Let us first discuss the voltammogram for the $Pb/EAC2/PbSO_4$ electrode. In the potential region between −1.3 V and −0.93 V, a reaction of Pb^{2+} reduction to Pb proceeds. This reaction proceeds on the surface of EAC particles. In the potential region between −0.93 V and −0.7 V, Pb is oxidized yielding $PbSO_4$ and an anodic peak appears. Possibly, some $Pb(OH)_2$ is also formed in the inner parts of the electrode where the movement of the H_2SO_4 flow through the $PbSO_4$ and the EAC layers is impeded. During the cathodic sweep from −0.77 V, cathodic current flows generated by the discharge of the double electric layer and by the reduction of $Pb(OH)_2$, if any. At potentials more negative than −0.93 V, reduction of $PbSO_4$ to Pb starts on the EAC surface, which results in a cathodic minimum. Occurrence of both anodic and cathodic peaks confirms the proposed parallel mechanism assuming that the electrochemical reaction of reduction of Pb^{2+} ions to Pb proceeds on the surface of the EAC2 particles.

Let us now consider the voltammograms for model electrodes with EAC3 additive. The charge and discharge voltammograms for the Pb/EAC3 electrode are similar to those for the double electric layer, but with significant hysteresis between the anodic and cathodic curves. Probably, an electrochemical reaction of hydrogen evolution proceeds and the evolved hydrogen is intercalated into the EAC3 phase. These hydrogen reactions yield increased hysteresis in the voltammograms. On the $Pb/EAC3/PbSO_4$ electrode, reactions of $PbSO_4$ reduction to Pb and of Pb oxidation to $PbSO_4$ proceed on the surface of the EAC3 particles. The over-potential at which oxidation of Pb to $PbSO_4$ starts is −0.91 V and reduction of $PbSO_4$ to Pb commences at almost the same potential. Above −1.20 V, intense evolution of hydrogen starts. A comparison between the voltammograms for the $Pb/EAC2/PbSO_4$ and the $Pb/EAC3/PbSO_4$ electrodes evidences stronger currents and more intense H_2 evolution for the latter electrode. These results indicate that the electrochemical reactions that proceed on the EAC surface depend very much on the type of the EAC additive used.

The model electrodes $Pb/EAC1/PbSO_4$ and $Pb/EAC4/PbSO_4$ have analogous behaviour to the one illustrated in Fig. 25.

4. Conclusions

Within the present study it has been established experimentally that the electrochemical reaction of reduction of lead ions proceeds simultaneously on the surface of both Pb and carbon particles. For the purpose of this investigation negative plates were prepared with addition of four types of electrochemically active carbon materials added in 5 different concentrations. Reference negative plates with no carbon additive were also prepared. The obtained negative active mass was characterized in terms of specific surface area, mean pore radius, structure and morphology of the crystals in NAM. These plates were assembled in test cells, which were set to capacity and cycling tests under simulated HRPSoC conditions. The cycling program comprised 1-min charge and discharge pulses with a current of 2*C* A. In the HRPSoC cycling mode, small $PbSO_4$ crystallites of high solubility are formed during charge with such high currents. Hence, during the subsequent discharge, dissolution of $PbSO_4$ proceeds at high rate. Thus a high concentration of Pb^{2+} ions is sustained in the NAM pores, so this first elementary process does not limit the rate of charge of the negative plates. Diffusion of Pb^{2+} ions to the surface of Pb particles is fast due to the high Pb^{2+} concentration gradient in the solution filling the pores resulting from the charge reaction. So this elementary process, too, is fast and does not limit the charge rate.

During charge, the potential of the negative plates with EAC additives is by 300–400 mV lower than the charge potential of plates with no carbon additives. This indicates that the transfer of electrons for the electrochemical reaction $Pb^{2+} + 2e^- \rightarrow Pb$ on the EAC surface proceeds with less hindrances than on the Pb surface. Hence, the cycle life performance of the cell will depend on the ratio EAC:Pb surface. The test results show that the longest cycle life is achieved when the cells contain EAC of the type and amount yielding NAM specific surface area of up to 4 m^2 g^{-1}. This effect of EAC is attributed to the nature of the EAC/solution interface and to the increased surface on which the electrochemical reaction $Pb^{2+} + 2e^- \rightarrow Pb$ proceeds. Thus, *electrochemically active carbons have a catalytic effect on the charge reactions* and reduction of $PbSO_4$ proceeds via *a parallel mechanism* on both Pb and EAC surfaces, which retards sulfation of the negative plates and prolongs the cycle life of the cells. The obtained polarization curves and the SEM images of the surface of NAM covered by EAC particles suggest that Pb atoms tend to incorporate in the growing Pb crystal lattice more easily than to form new nuclei on foreign substrate.

The proposed parallel mechanism of $PbSO_4$ reduction on the EAC and Pb surfaces was verified experimentally using specially designed model electrodes. Apart from the parallel electrochemical mechanism of $PbSO_4$ reduction to Pb, electrochemically active carbons influence also the pore structure of NAM reducing its mean pore radius. When the pores "shrink" to less than 1.5 μm, access of H_2SO_4 into the pores is impeded and PbO forms instead of $PbSO_4$ during cell discharge, i.e. the overall electrochemical reaction of charge and discharge of the negative plates changes.

Identification of the above-mechanism of action of carbon additives on the performance of lead-acid batteries operated in the HRPSoC mode opens the way to development of new technological processes for battery manufacture, which would improve the reversibility of the processes during HRPSoC cycling and thus make lead-acid batteries suitable and widely acceptable for HEV applications.

Acknowledgements

The authors acknowledge with gratitude the financial support provided by the Advanced Lead-Acid Battery Consortium and the valuable discussions with Dr. P. Moseley in the course of carrying out the present investigation. This paper was reported at the ALABC Technical Meeting held within the LABAT'2008 conference.

References

[1] K. Nakamura, M. Shiomi, K. Takahashi, M. Tsubota, J. Power Sources 59 (1996) 153.
[2] M. Shiomi, T. Funato, K. Nakamura, K. Takahashi, M. Tsubota, J. Power Sources 64 (1997) 147.
[3] A.F. Hollenkamp, W.G.A. Baldsing, S. Lau, O.V. Lim, R.H. Newnham, D.A.J. Rand, J.M. Rosalie, D.G. Vella, L.H. Vu, ALABC Project N1.2, Overcoming negative-plate capacity loss in VRLA batteries cycled under partial-state-of-charge duty. Final Report, Proceedings of Advanced Lead-Acid Battery Consortium, Research Triangle Park, NC, USA, 2002.
[4] P.T. Moseley, R.F. Nelson, A.F. Hollenkamp, J. Power Sources 157 (2006) 3.
[5] R.H. Newnham, W.G.A. Baldsing, A.F. Hollenkamp, O.V. Lim, C.G. Phyland, D.A.J. Rand, J.M. Rosalie, D.G. Vella, ALABC Project C/N1.1, Advancement of valve-regulated lead-acid battery technology for hybrid-electric and electric vehicles. Final Report, Proceedings of Advanced Lead-Acid Battery Consortium, Research Triangle Park, NC, USA, 2002.
[6] P.T. Moseley, J. Power Sources 191 (2009) 134–138.
[7] L.T. Lam, C.G. Phyland, D.A.J. Rand, D.G. Vella, L.H. Vu, ALABC Project N3.1. Final Report, Proceedings of Advanced Lead-Acid Battery Consortium, Research Triangle Park, NC, USA, 2002.
[8] L.T. Lam, R. Louey, J. Power Sources 158 (2006) 1140.
[9] L.T. Lam, R. Louey, N.P. Haigh, O.V. Lim, D.G. Vella, C.G. Phyland, L.H. Vu, J. Furukawa, T. Takada, D. Monma, T. Kano, J. Power Sources 174 (2007) 16.
[10] D. Pavlov, V. Iliev, J. Power Sources 7 (1981) 153.
[11] G. Petkova, D. Pavlov, J. Power Sources 113 (2003) 355.